

A Novel Coal Fly Ash Sphere Reveals a Complete Understanding of Plerosphere Formation

Patrick S. Chepaitis, James R. Millette and Tim B. Vander Wood
MVA Scientific Consultants, Inc.*

KEYWORDS

Backscattered electron imaging (BEI), cenosphere, coal combustion, fly ash, plerosphere, scanning electron microscopy (SEM), secondary electron imaging (SEI), X-ray energy dispersive spectrometry (EDS)

ABSTRACT

The mechanism of formation of a plerosphere, a type of coal fly ash particle that contains microspheres, has proven difficult to describe, especially when considering the role of the hollow spheres named cenospheres. Thirteen fly ash samples were studied using scanning electron microscopy (SEM) and X-ray energy dispersive spectrometry (EDS) in order to gather new information about the basic mechanism. The identification and study of thin-walled cenospheres provides key evidence in support of a previously proposed theory in which plerospheres are formed by the capture of smaller fly ash spheres after implosion of cenospheres.

INTRODUCTION

Since coal combustion began as a procedure for power generation, significant amounts of ash have been produced. The steps through which coal combusts, typically in an electric power plant furnace or boiler, are well known. Just as well known is the fact that this combustion generates coal combustion byproducts (CCBs). Bottom ash, the non-combustible portions of

coal that sticks to the furnace walls or fall to the bottom of an ash hopper, and boiler slag, which is bottom ash that has been quenched with water, are two such CCBs. After the flue gas has left the boiler, particulate collection devices such as electrostatic precipitators, may collect fine, powdery fly ash as another combustion product.

Fly ash particles have been characterized by light microscopy (1) and scanning electron microscopy (2). Among the least well-understood fly ash particles are the cenospheres and plerospheres that are typically present, to some degree, in fly ash samples. Cenospheres are hollow, glassy spheres, while plerospheres contain additional spheres or ash particles that are visible upon the destruction of the outer shell. Two general mechanisms for plerosphere formation have been proposed. Fisher et al. introduced the most widely accepted mechanism for plerosphere formation (3) — the core of a sphere boils away inside the shell due to the development of a temperature gradient, leading to the production of spherical particles inside the shell upon cooling. In this mechanism, plerospheres are the precursors of cenospheres (4). The second mechanism for plerosphere formation (5) is much simpler. Shibaoka and Paulson propose that after a cenosphere has ruptured or collapsed due to differences in internal gas pressure, microspheres in the turbulent flue gas become entrained inside the broken cenospheres. Goodarzi and Sanei (6) have advanced an additional proposal for plerosphere formation that deals with secondary plerosphere formation, combining the ideas of Fisher and Shibaoka. The identification

*3300 Breckinridge Boulevard, Suite 400, Duluth, GA 30096

Table 1. Fly Ash Sample Descriptions

Sample No.	Location	Description	SEM Coating
W0017	Unknown	#15-16 Fly Ash	C
W0020	Jeffrey Energy Center, St. Mary, KS	Class C Fly Ash	Au
W0021	Tecumseh Energy Center, Topeka, KS	Fly Ash	Au
W0022	Unknown	BLR #12 Coal Base Fly Ash	C
W0023	Unknown	BLR #15-16 Coal Base Fly Ash	Au
W0043	Public Service Co., Bow, NH	Fly Ash	C
W0068	Great River Energy, Lignite, ND	Fly Ash	C, Au
W0084	Southern Illinois Power Cooperative, Marion, IL	Unit 4 Fly Ash	C
W0085	Southern Illinois Power Cooperative, Marion, IL	Unit 123 Fly Ash	Au
W0109	Gavin Power Plant, Cheshire, OH	Fly Ash	Au
W0110	PPL Montour, Washingtonville, PA	Fly Ash	None
W0111	Zimmer Power Station Moscow, OH	Fly Ash	Au
W0112	Clifty Creek Power Plant, Madison, IN	Fly Ash	Au

of a novel fly ash particle found in the authors' study provides new evidence for the mechanism of plerosphere formation.

MATERIALS AND METHODS

We analyzed 13 fly ash samples from a wide range of locations in the United States (Table 1) by SEM together with EDS. Preparation for SEM involved scattering a portion of each fly ash sample onto double-sided carbon sticky tape mounted on an aluminum SEM stub. The samples were then either coated with carbon or gold. We performed SEM analyses with secondary electron imaging (SEI) and backscattered electron imaging (BEI) at accelerating voltages of 15 kV and 20 kV using a JEOL JSM-6490LV SEM. We utilized a Thermo Scientific Noran System SIX X-ray dispersive spectrometer for elemental analysis.

RESULTS

Typical aluminosilicate fly ash spheres (Figure 1) were identified in 12 of 13 samples. Cenospheres (Figure 2) and plerospheres (Figure 3) were found in more than half of the samples. Coal and char particles were also found, although for the majority of the samples these particles were rare.

Eight out of the 13 fly ash samples contained a newly identified type of fly ash sphere. This new sphere (Figure 4, page 178) termed "thin-walled cenosphere" consists of two regions: the more abundant brighter region of the sphere and a darker region proposed as an incipient collapse zone. EDS spectra of the normal zone and the incipient collapse zone are also shown in Figure 4. Compositional analysis results are given in Table 2 (page 179). Figure 5 (page 179) shows a thin-walled cenosphere viewed at accelerating voltages of

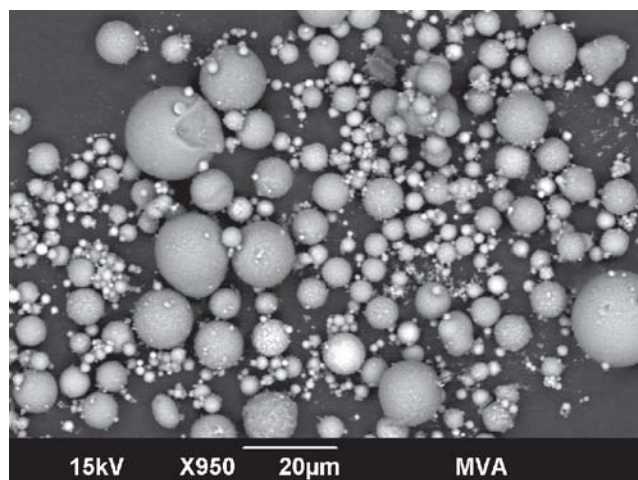


Figure 1. A backscattered electron image of fly ash spheres.

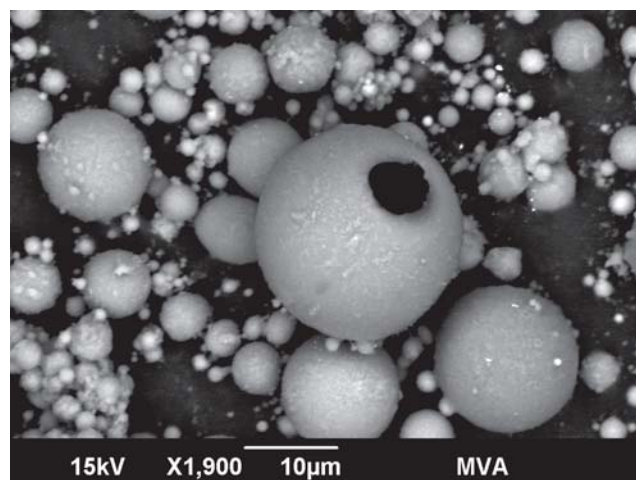


Figure 2. A backscattered electron image of a cenosphere.

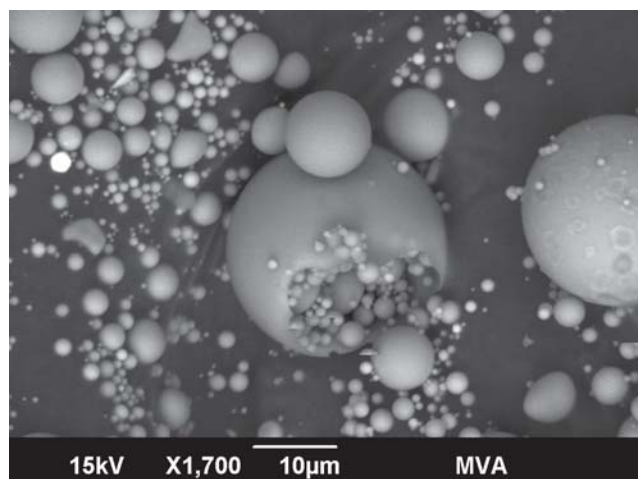


Figure 3. A backscattered electron image of a plerosphere.

15 kV and 20 kV, using either SEI or BEI and viewed at a tilt of approximately 15° and a rotation of 90° .

DISCUSSION AND CONCLUSIONS

We propose that the dark area of the cenosphere is in fact a thin spot in the cenosphere's shell that leads to collapse. However, charging, geometry effects and compositional differences, in addition to the proposed sample thickness difference, may also cause the observed contrast. Coating the samples with either gold or carbon minimized charging, and we did not observe any characteristic contrast effects. The contrast and orientation were consistent at various accelerating voltages and in backscattered and secondary images (Figure 5a–5d). Geometry contrast effects arise from the orientation of the sample relative to the electron

beam and detector. Observation of the dark regions during rotation and tilting of the specimen indicated that these regions were fixed relative to the sphere's surface and not dependent on orientation (Figure 5e–5f). This suggests that the dark regions arise from a property intrinsic to the sphere and not the geometry of the analysis. The results of compositional analysis (Figure 4) indicate that the observed contrast is not due to difference in elemental composition. The final contrast mechanism that could account for this dark spot is the thickness of the sphere at that location. Contrast due to thin film thickness variation has been studied previously (7, 8, 9). The dark region that we observed on the cenospheres is consistent with a thinner area of the hollow cenosphere wall.

The mechanism proposed here and outlined in Figure 6 (page 180) is consistent with that proposed by Shibaoka and Paulson. The process begins when cenospheres leave the hot zone and re-enter the turbulent flue gas. The temperature and pressure inside the newly formed cenosphere decrease significantly. The cenosphere (Figure 6a) begins to collapse at the thin, dark region after leaving the hot zone as the internal pressure continuously falls. After implosion in the swirling flue gas (Figure 6b), microspheres become entrained in the broken cenosphere (Figure 6c), as Shibaoka and Paulson have proposed. The depressed lip of the void of the plerosphere, observable in the plerosphere image of Figure 6c (and also in Figure 2 and Figure 3), also provides evidence for implosion.

SEM analyses of 13 unique fly ash samples suggests a better explanation for plerosphere formation. Combining key elements of Shibaoka and Paulson's (5) study with the identification of a new fly ash sphere — the thin-walled cenosphere — the authors propose that

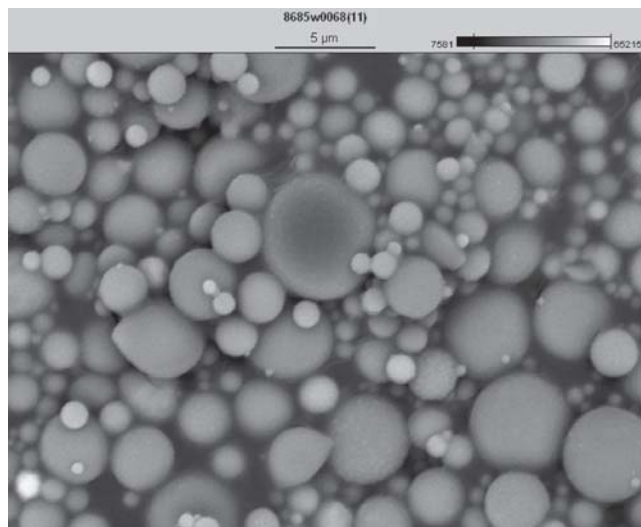
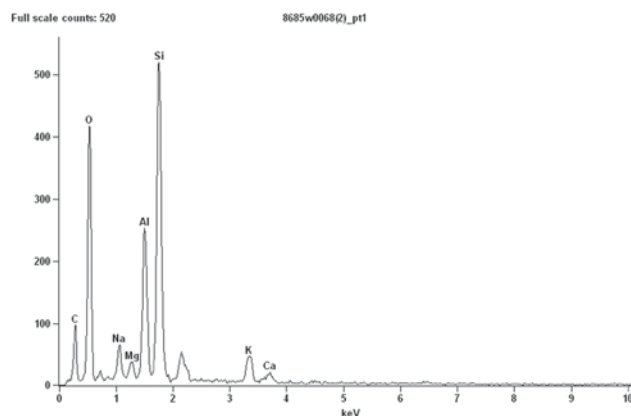
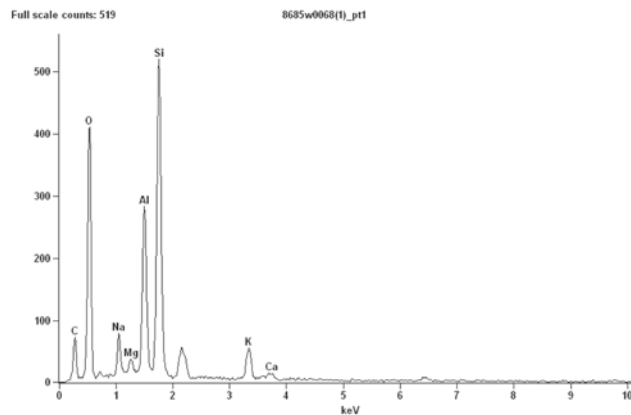


Figure 4. Above: A backscattered electron image of a thin-walled cenosphere. Right: EDS spectra of the normal zone (top) and incipient collapse zone (bottom).



plerospheres are formed upon collapse of thin-walled regions of the cenospheres as temperature decreases in the flue gas cause pressure decreases within the spheres. Smaller spheres then simply become trapped inside the broken cenosphere leading to a plerosphere.

ACKNOWLEDGMENTS

Lead author P.S. Chepaitis, an intern from Georgia Institute of Technology, would like to thank J.R. Millette and T.B. Vander Wood for mentorship throughout the writing and experimental processes of this publication. The authors would also like to thank R.S. Brown of MVA Scientific Consultants for his help in experiments dealing with thin-film thickness contrast on the SEM.

REFERENCES

1. Fisher, G.L., Prentice, B.A., Silberman, D., Ondov, J.M., Biermann, A.H., Ragalni, R.C. and McFarland, A.R. "Physical and Morphological Studies of Size-Classified Coal Fly Ash," *Environmental Science & Technology*, **12**, pp 447–451, 1978.
2. Kutchko, B.G. and Kim, A.G. "Fly ash characterization by SEM-EDS," *Fuel*, **85**, pp 2537–2544, 2006.
3. Fisher, G.L., Chang, D.P.Y. and Brummer, M. "Fly Ash Collected from Electrostatic Precipitators: Microcrystalline Structures and the Mystery of the Spheres," *Science*, **192**, pp 553–555, 1976.
4. Fenelonov, V.B., Mel'gunov, M.S. and Parmon,

V.N. "The Properties of Cenospheres and the Mechanism of Their Formation During High-Temperature Coal Combustion at Thermal Power Plants," *KONA Powder and Particle Journal*, **28**, pp 189–208, 2010.

5. Shibaoka, M. and Paulson, A.J. "Genesis of char and ash plerospheres," *Fuel*, **65**, pp 1020–1022, 1986.

6. Goodarzi, F. and Sanei, H. "Plerosphere and its role in reduction of emitted fine fly ash particles from pulverized coal-fired power plants," *Fuel*, **88**, pp 382–386, 2009.

7. Kita, Y., Kasai, Y., Hashimoto, S., Iiyama, K., Takmiya, S. "Application of Brightness of Scanning Electron Microscope Images to Measuring Thickness of Nanometer-Thin SiO₂ Layers on a Si Substrates," *Japanese Journal of Applied Physics*, **40**, pp 5861–5864, 2001.

8. Suzuki, M., Kumagai, K., Sekiguchi, T., Cassell, A.M., Saito, T. and Yang, C.Y. "Secondary electron emission from freely supported nanowires," *Journal of Applied Physics*, **104**, pp 114306-1–114306-6, 2008.

9. Suzuki, M., Ominami, Y., Sekiguchi, T. and Yang, C.Y. "Secondary electron imaging of embedded defects in carbon nanofiber via interconnects," *Applied Physics Letters*, **93**, pp 263110-1–263110-3, 2008.

Table 2. EDS Elemental Compositional Analysis*

Composition	Normal Zone (Weight %)	Incipient Collapse Zone (Weight %)
C	10.39+ / -0.44	10.74+ / -0.42
O	44.03+ / -0.86	40.08+ / -0.83
Na	2.92+ / -0.24	2.7+ / -0.16
Mg	0.99+ / -0.17	1.26+ / -0.15
Al	10.93+ / -0.35	10.91+ / -0.39
Si	25.54+ / -0.34	27.76+ / -0.54
K	4.03+ / -0.36	4.81+ / -0.23
Ca	1.17+ / -0.19	1.74+ / -0.21

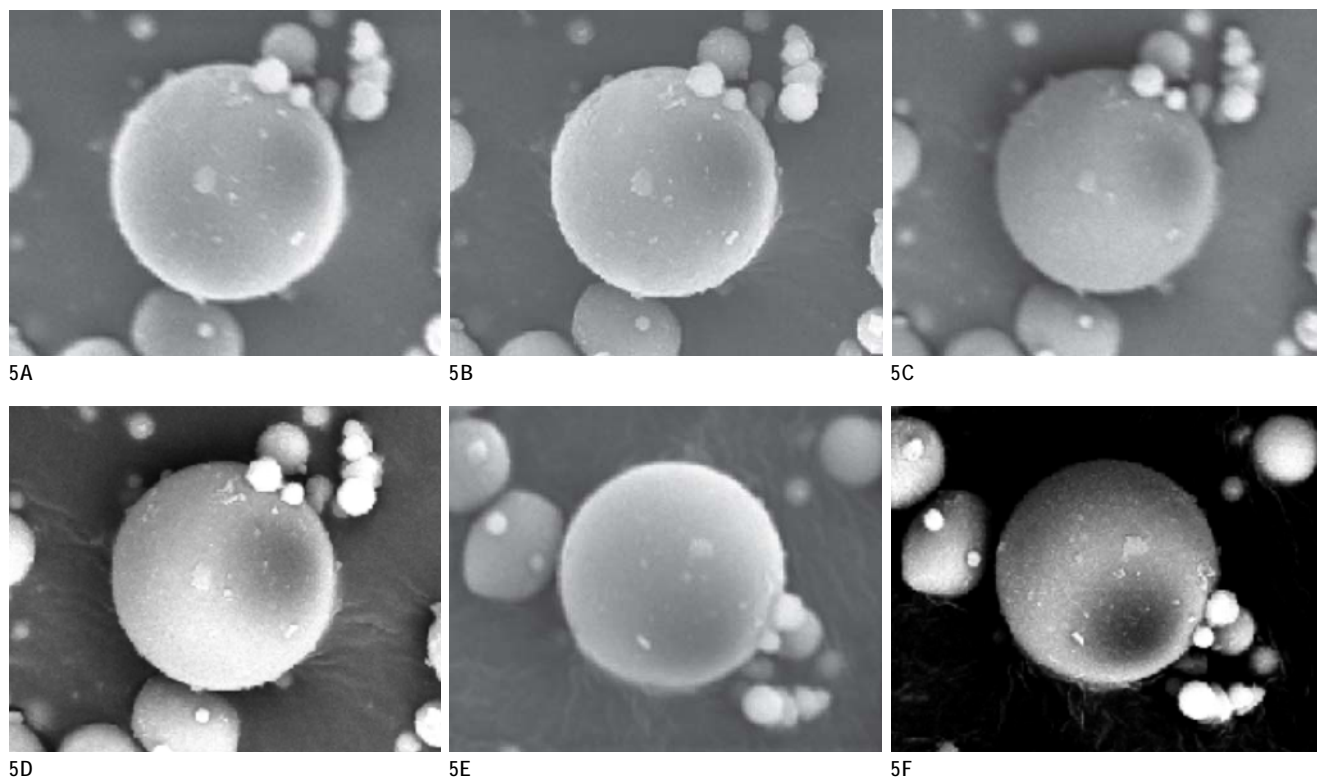
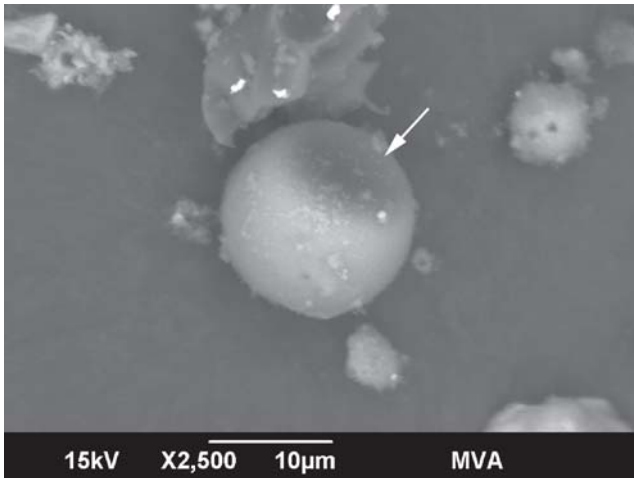
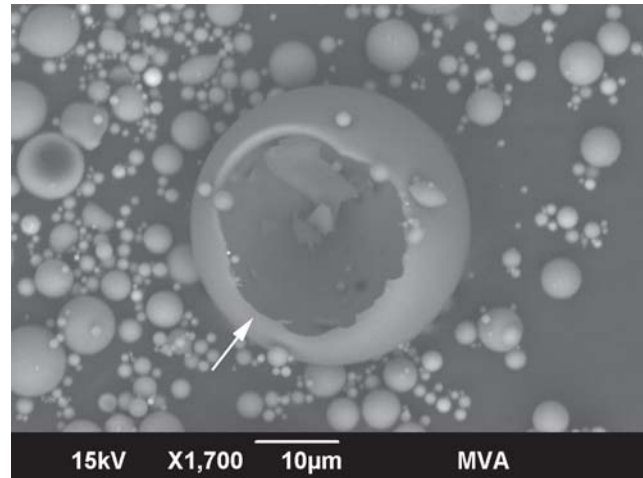
*Uncertainty is 1σ .

Figure 5. SEM images show the same 20 μm diameter thin-walled cenosphere at different accelerating voltages and image modes. 5A, secondary electron image (SEI) at 15 kV; 5B, SEI image at 20 kV; 5C, backscattered electron image (BEI) at 15 kV; 5D, BEI at 20 kV; 5E, SEI image at 20 kV, rotation = 90.047° , tilt = 15° ; and 5F, BEI image at 20 kV, rotation = 90.047° , tilt = 15° .

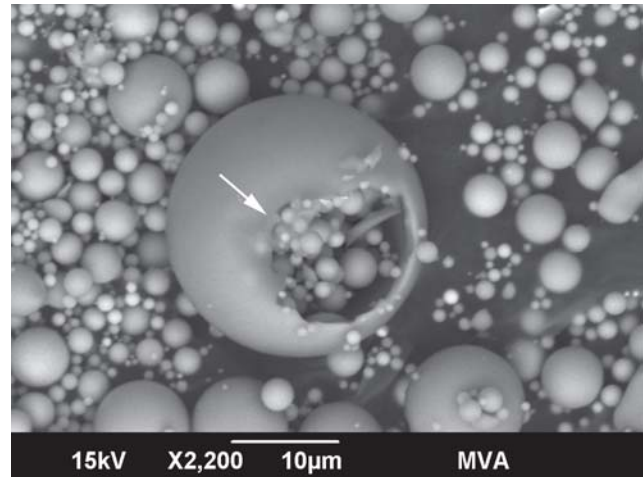


6A



6B

Figure 6. Backscattered electron and secondary electron images of a proposed plerosphere formation mechanism show: 6A, a newly identified thin-walled cenosphere with a collapse zone (arrow); 6B, a collapsed cenosphere (arrow); and 6C, a plerosphere, with a depressed collapse region (arrow), forming within swirling flue gas.



6C